Different temperature- and pressure-effects on the water-mediated interactions between hydrophobic, hydrophilic, and hydrophobic-hydrophilic nanoscale surfaces *⊙*

Special Collection: Fluids Meet Solids

Justin Engstler 📵 ; Nicolas Giovambattista 🗷 📵



J. Chem. Phys. 157, 064701 (2022) https://doi.org/10.1063/5.0097908

> View Online



CrossMark



The Journal of Chemical Physics

Special Topic: Adhesion and Friction

Submit Today!





Different temperature- and pressure-effects on the water-mediated interactions between hydrophobic, hydrophilic, and hydrophobic-hydrophilic nanoscale surfaces

Cite as: J. Chem. Phys. 157, 064701 (2022); doi: 10.1063/5.0097908

Submitted: 3 May 2022 • Accepted: 7 July 2022 •

Published Online: 8 August 2022









Justin Engstler^{1,a)} and Nicolas Giovambattista^{2,3,b)}



AFFILIATIONS

- M. S. Program in Nanoscience, The Graduate Center of the City University of New York, New York, New York 10016, USA
- Department of Physics, Brooklyn College of the City University of New York, Brooklyn, New York 11210, USA
- ³ Ph.D. Programs in Chemistry and Physics. The Graduate Center of the City University of New York. New York, New York 10016, USA

Note: This paper is part of the JCP Special Topic on Fluids Meets Solids.

^{a)}jtpve921@gmail.com

b) Author to whom correspondence should be addressed: ngiovambattista@brooklyn.cuny.edu

ABSTRACT

Water-mediated interactions (WMIs) are responsible for diverse processes in aqueous solutions, including protein folding and nanoparticle aggregation. WMI may be affected by changes in temperature and pressure, and hence, they can alter chemical/physical processes that occur in aqueous environments. Traditionally, attention has been focused on hydrophobic interactions while, in comparison, the role of hydrophilic and hybrid (hydrophobic-hydrophilic) interactions have been mostly overlooked. Here, we study the role of T and P on the WMI between nanoscale (i) hydrophobic-hydrophobic, (ii) hydrophilic-hydrophilic, and (iii) hydrophilic-hydrophobic pairs of (hydroxylated/non-hydroxylated) graphene-based surfaces. We find that hydrophobic, hydrophilic, and hybrid interactions are all sensitive to P. However, while hydrophobic interactions [case (i)] are considerably sensitive to T-variations, hydrophilic [case (ii)] and hybrid interactions [case (iii)] are practically T-independent. An analysis of the entropic and enthalpic contributions to the potential of mean force for cases (i)-(iii) is also presented. Our results are important in understanding T- and P-induced protein denaturation and the interactions of biomolecules in solution, including protein aggregation and phase separation processes. From the computational point of view, the results presented here are relevant in the design of implicit water models for the study of molecular and colloidal/nanoparticle systems at different thermodynamic conditions.

Published under an exclusive license by AIP Publishing. https://doi.org/10.1063/5.0097908

I. INTRODUCTION

Water-mediated interactions (WMIs) are fundamental forces that drive molecular processes in aqueous solutions, including protein aggregation and interactions, 1,2 the formation of membranes and micelles,^{3–5} protein folding,^{6,7} and molecular recognition.^{8,9} At the nanoscale, WMIs are complex and difficult to predict since they are inherently dependent on the properties of the interacting surfaces, such as the surface chemistry, curvature, polarity, and

distribution of partial charges.¹⁰ The most studied and relevant kind of WMI is the hydrophobic interaction. 4,5,11,12 However, the WMI between hydrophilic surfaces (hydrophilic interactions) and between a pair of hydrophilic-hydrophobic surfaces (hybrid interactions) may also play a relevant role. After all, typical protein surfaces are rather heterogeneous with hydrophobic and hydrophilic domains exposed to the surrounding water.¹³ A few studies show that hydrophilic interactions can indeed play a relevant role in driving molecular processes in aqueous environments.

In a recent study, ¹⁹ we explored in detail the WMIs between (i) hydrophobic-hydrophobic, (ii) hydrophilic-hydrophilic, and (iii) hydrophobic-hydrophilic pairs of nanoscale plates at P = 0 MPa and T = 300 K. The forces between the plates in cases (i)-(iii) were all comparable; hence, they should all play a relevant role in driving a self-assembly system toward its final state. However, the hydrophobic interactions [case (i)] were found to be more effective in providing stability to self-assembled systems. The aim of this work is to extend the studies of Ref. 19, based on graphenebased hydrophobic and hydrophilic nanoscale plates, to include the effects of temperature and pressure. The rationale of doing so is simple. Changes in the working conditions, such as temperature and pressure, can alter the behavior of nanoconfined water,²³ which, in turn, may also alter the WMIs between interacting surfaces. Indeed, hydrophobic interactions are very sensitive to both temperature and pressure variations. 24,25 The effects of temperature and pressure on molecular processes occurring in aqueous solutions are nicely exemplified by the common phase behavior of proteins. Proteins that are stable (folded) at normal conditions can denature (unfold) by isothermal compression/decompression and isobaric heating/cooling.20

This work is organized as follows: In Sec. II, we describe the computer simulations details. The results are included in Sec. III, where we discuss the temperature- and pressure-effects on the mean force and potential of mean force (PMF) between (i) hydrophobic-hydrophobic, (ii) hydrophilic-hydrophilic, and (iii) hydrophobic-hydrophilic pairs of surfaces. Also included in Sec. III is a discussion of the entropic and enthalpic contributions to the PMF found in the systems studied. A summary and discussion are included in Sec. IV.

II. COMPUTER SIMULATIONS DETAILS

We perform molecular dynamics (MD) simulations of three different systems consisting of two graphene-based nanoscale *plates* immersed in water; see Figs. 1(a) and 1(b). Three different systems are considered containing (a) two hydrophilic plates [Fig. 1(c)], (b) two hydrophobic plates [Fig. 1(d)], or (c) one hydrophobic and one hydrophilic plate [Figs. 1(a) and 1(b)]. These systems will be used to compare the effects of T and P on the plate–plate (a) hydrophobic, (b) hydrophilic, and (c) hybrid (hydrophobic/hydrophilic) interactions. In order to study the role of temperature on the corresponding WMIs, MD simulations are performed at P = 0 MPa for T = 240, 260, 280, 300, 360, and 400 K, below and above the melting temperature of water. Similarly, in order to study the effects of pressure on the target WMIs, MD simulations are performed at T = 300 K for different pressures in the range $-120 \le P \le 2000$ MPa.

Figure 1(a) shows the system used to study T-effects on the WMIs between the plates. The MD simulations are performed at constant volume, temperature, and number of water molecules, N = 7924. The plates are located at fixed positions parallel to the xy-plane, symmetrically about the center of the simulation box. The system box dimensions are $L_x = 6.0$ nm, $L_y = 15.0$ nm, and $L_z = 7.0$ nm, and periodic boundary conditions apply along the x-, y-, and z-directions. The water bath expands across the system along the x- and z-directions. Along the y-direction, an empty space is left above and below the water bath so the pressure of the system

can be maintained at P = 0 without the use of a barostat; see Ref. 19 for details

Figure 1(b) shows the system used to study P-effects on the WMI between the plates. This is the same system shown in Fig. 1(a) with the water bath being sandwiched by two large graphene walls separated by a distance $\Delta y < L_y$. As for the plates, the graphene walls remain immobile throughout the MD simulation. Although the MD simulations are performed at constant (N, V, T) conditions, one can control the pressure of the water-plates system by varying the value of Δy . Figure S1 of the supplementary material shows the pressure on the upper and bottom walls as function of Δy ; $P(\Delta y)$ is well behaved and, in particular, independent of the plates considered. In the MD simulations, *P* is calculated by evaluating the average forces produced by the water molecules on each wall, divided by the wall surface area $S = L_x \times L_z$. In principle, one could avoid using the two graphene walls shown in Fig. 1(b) to control the pressure of the water-plates system by performing MD simulations at constant (N, P, T) (for a system composed of the two plates of interest immersed in water with no graphene walls). However, nonzero interactions between the atoms in the plates can lead to an incorrect calculation of the pressure of the system and, hence, affect the barostat performance. In the case of graphene plates, where the C atoms have no charge, the plate-plate interactions can be removed by zeroing the C-C [Lennard-Jones (LJ)] interactions (see, e.g., Ref. 24). However, removing the plate-plate interactions for plates that have nonzero atomic partial charges, which is the case of this work, can be cumbersome due to long range electrostatic interactions. By controlling the pressure of water using the upper and lower graphene walls shown in Fig. 1(b), we can avoid these technical issues. As shown in the supplementary material, our simulations using the configuration shown in Fig. 1(b) for the case of apolar (graphene) plates are fully consistent with the results obtained in Refs. 19 and 25.

Water molecules are represented by using the TIP4P/2005 model;³⁰ the plates are modeled after graphene. Figures 1(c) and 1(d) show the two kinds of plates considered in this work, G-plates and HOG-plates. The G-plates correspond to graphene and are composed of C atoms that interact only with water O atoms via Lennard-Jones interactions.²⁴ The HOG-plates are constructed by hydroxylating one side of the G-plate; the OH groups of these plates always face the confined water volume. The HOG-plates atoms have partial charges and can form hydrogen bonds (HB) with water. While the G-plates are weakly hydrophobic (with a water contact angle of $\theta_c \approx 96^{\circ}$), the HOG-plates are hydrophilic ($\theta_c \approx 0$). Both the G- and HOG-plates have nanoscale dimensions with a surface area $A = d_x \times d_y = 1.832 \times 1.974 \text{ nm}^2$. The structure of these plates and the plate-water interactions (including the plate atoms' partial charges and Lennard-Jones parameters) are described in detail in Ref. 19.

Our study is based on the calculation of the potential of mean force (PMF) between the plates at a given temperature and pressure. To calculate the PMF, we perform MD simulations with the plates separated by a distance r (values of r are in the range 0.2–1.8 nm, depending on the plates considered, and vary in increments of $\Delta r = 0.02$ nm). From the MD simulation, we extract the mean force F(r) acting on the plates from which the PMF is calculated by simple integration; see details in Refs. 19 and 24. For a given state point (T, P) and plate separation r, MD simulations are

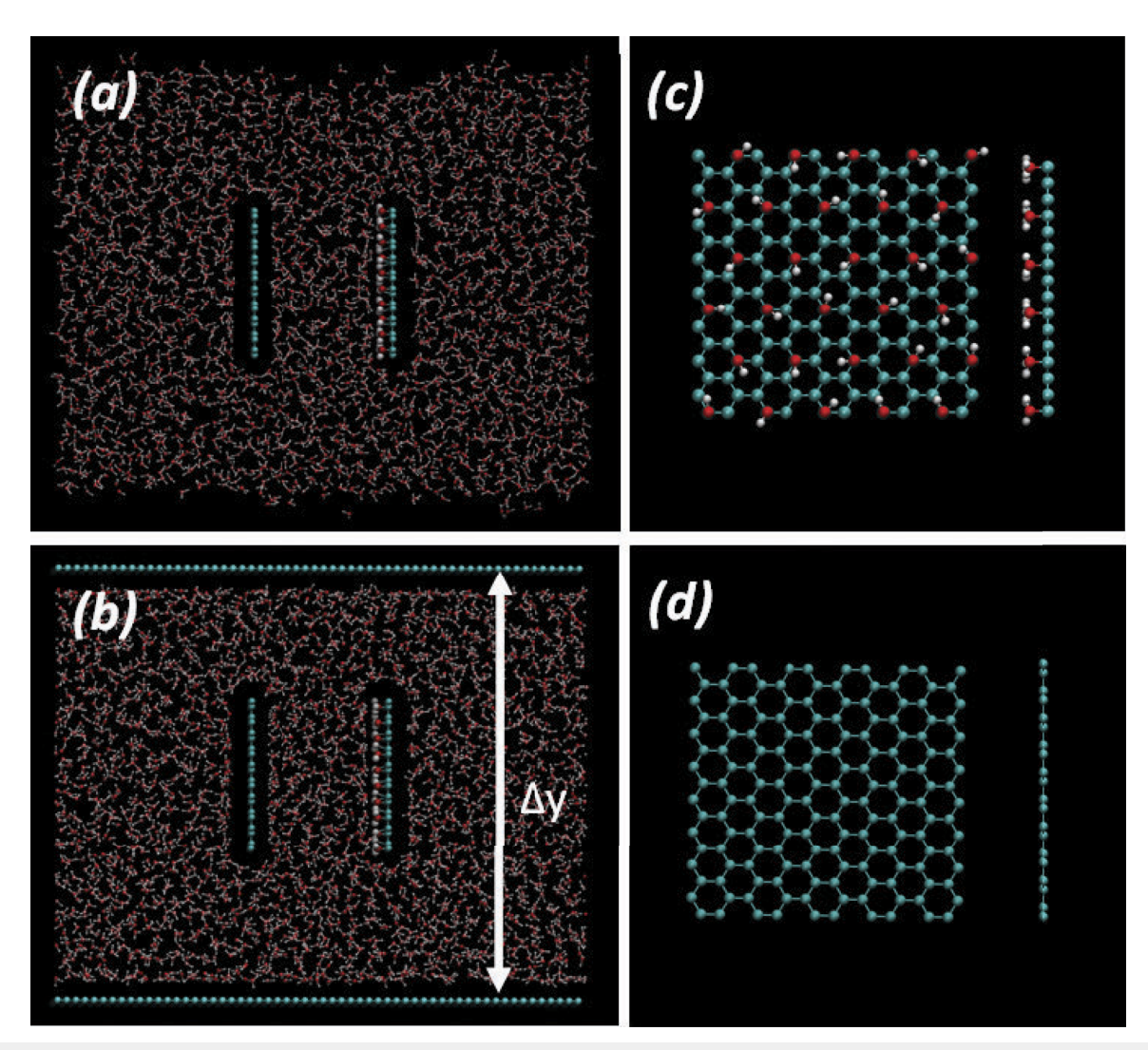


FIG. 1. (a) System configuration employed to study the effects of *temperature* on the WMIs between nanoscale plates at constant pressure (P=0). Cross section of a system composed of a graphene (left) and a hydroxylated graphene plate (right) immersed in water (the plates separation is r=1.50 nm). Plates are located symmetrically about the center of the box, parallel to the xy-plane, and periodic boundary conditions apply along all three directions. An empty space along the vertical y axis (not shown) is included to maintain the pressure of the system at P=0 MPa. (b) System configuration employed to study the effects of *pressure* on the WMIs between nanoscale plates at constant temperature (T=300 K). The system is similar to that shown in (a) but includes two large graphene walls sandwiching the water–plates system. By controlling the separation Δy between the walls, one can control the pressure of the water–plates system; see the supplementary material [in (b), $\Delta y=5.8$ nm, which corresponds to $P\approx0$]. (c) Front and side views of the hydrophilic plates used in this work (HOG-plate) obtained by hydroxylating one side of a graphene plate. (d) Front and side views of the graphene plates (G-plates) used in this work.

performed for 4 ns using a time step dt = 0.002 ps. Data analysis is performed based on the last 2–3 ns of the simulation runs (see Ref. 19). The total simulation times appear to be long enough to avoid nonequilibrium artifacts in our measurements at all temperatures. For comparison, we note that the time τ_{bulk} at which the mean-square displacement of the water molecules in the bulk liquid reaches the value $\approx 1 \text{ nm}^2$ is relatively short at T = 400 - 240 K (τ_{bulk} is roughly equal to few times the structural relaxation time of the liquid measured, e.g., from the intermediate scattering

function³¹). For TIP4P/2005 water at $\rho = 1.0$ g/cm³, we find that $\tau_{bulk} = 74$ and 746 ps at T = 400 and 240 K, respectively. Hence, even at our lowest temperature (T = 240 K), the simulation time is more than five times τ_{bulk} . It could still be possible that at very short plates separations, the confined liquid is metastable relative to the vapor. ^{32–34} However, as we showed in Ref. 19, for the case of HOG-HOG plates, the PMF is practically independent on whether water is initially placed within the confined space (wet initial conditions) or artificially removed between the plates (dewetted initial

conditions). Similarly, we confirm that the PMF between the G-G plates is unaffected by the initial conditions considered. Specifically, we calculate the mean force between the G-G plates by performing MD simulations starting from a short plate separation r^* and increasing the values of r sequentially up to $r \le 0.74$ nm. As shown in the supplementary material, MD simulations starting from (i) $r^* = 0.30$ nm (dewetted initial condition), (ii) $r^* = 0.50$ nm (dewetted initial condition), and (iii) $r^* = 0.64$ nm (wet initial condition) produced practically indistinguishable results to those shown in Ref. 19 and Fig. 2(a).

All computer simulations are performed using the Gromacs software package.³⁵ The temperature is maintained constant by using a Nosé–Hoover thermostat with a time constant of 1 ps. Electrostatic interactions are treated using a particle mesh Ewald (PME) solver with a reciprocal space griding of 0.12 nm and cubic polynomial interpolation. A cutoff $r_c = 1.1$ nm is used for the real space force calculations of the PME solver, as well as for the LJ short-range interactions.

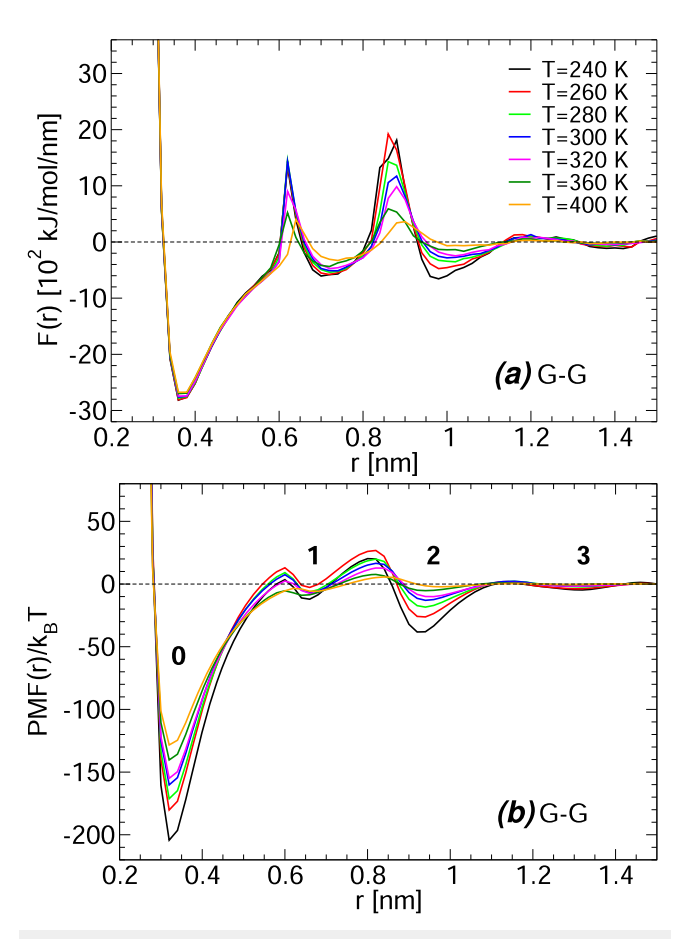


FIG. 2. (a) Mean force and (b) potential of mean force between G-G plates immersed in water at selected temperatures (P = 0 MPa); adapted from Ref. 24. Numbers in bold font in (b) indicate the number of water layers formed between the plates at the plates separations corresponding to the PMF minima. r is the distance between the planes containing the C atoms of the plates.

III. RESULTS

The results are organized as follows. In Secs. III A and III B, we address the effects of T on the WMIs between the target nanoscale plates and the corresponding entropic/enthalpic contributions. The effects of P are discussed in Sec. III C.

A. Temperature-effects

The effects of temperature on the WMIs between G-G plates were discussed in detail in Ref. 24. In that work, the pressure was controlled by using a Berendsen barostat with no graphene walls. The mean force F(r) and PMF G(r) between the G-G plates at different temperatures and at P = 0.1 MPa are shown in Fig. 2 (reproduced from Ref. 24). Briefly, both F(r) and G(r) are oscillatory functions of the plate-plate separation r. The local minima of the PMF, at r_0 , r_1 , r_2 , $r_3 = 0.32$, 0.67, 0.93, 1.31 nm, represent the stable/metastable states of the system. The deepest minimum of the PMF occurs at $r = r_0$ and corresponds to the stable plate-plate separation to which the system will be driven due to thermal fluctuations. Interestingly, the local minimum of the PMF at $r = r_n$ (n = 0, 1, 2, 3) corresponds to the plate separations at which the water molecules between the plates arrange into n layers. It follows that in the stable state of the system, $r = r_0$, the plates are in contact with each other (collapsed-plates state). The effect of cooling on the PMF between the G-G plates is to increase the free energy barriers that separate the stable/metastable states. Alternatively, the depth of the PMF local minima decreases upon heating. This means that increasing T weakens the hydrophobic interactions between the G-G plates. To confirm that these conclusions are general, i.e., common to hydrophobic surfaces other than graphene, we study in the supplementary material the mean force and PMF between two OG-plates. The OG-plates are apolar and are obtained from the HOG-plates by removing the H atoms and all partial charges (details on the structure of the OG-plates is given in Ref. 19). The F(r) and PMF for the case of two OG-plates show qualitatively similar T-effects to those shown in Fig. 2.

Next, we focus on the effects of temperature on the hydrophilic and hybrid interactions. The mean forces and PMF between the HOG-HOG and HOG-G plates obtained from our MD simulations are shown in Fig. 3. In both cases, the mean force and PMF are oscillatory functions of r. ¹⁹ As for the case of the G-G plates, the local minima of the PMF correspond to the formation of an integer number of water layers between the plates. Interestingly, in the case of HOG-HOG and HOG-G plate systems, there is no collapsedplates state and, instead, water is found in the confined volume at all plate separations r. The main point of Fig. 3 is that the WMIs between HOG-HOG and HOG-G plates are practically independent of temperature. Specifically, the mean forces between hydrophilic and hybrid plates are practically unaffected by changes in temperature [see Figs. 3(a) and 3(c)]. A comparison among Figs. 2(b), 3(b) and 3(d), shows that the T-effects on the PMF between HOG-HOG and G-HOG plates (in units of k_{BT}) are rather mild relative to the corresponding changes found in the PMF between G-G plates. It also follows from Fig. 3 that the presence of a single hydrophilic HOG-plate is sufficient to induce hydrophilic-like, practically Tindependent interactions, despite the hydrophilicity/hydrophobicity of the opposite surface.

The practically lack of temperature-effects on the PMF between the HOG-HOG and G-HOG plates may be rationalized in terms of

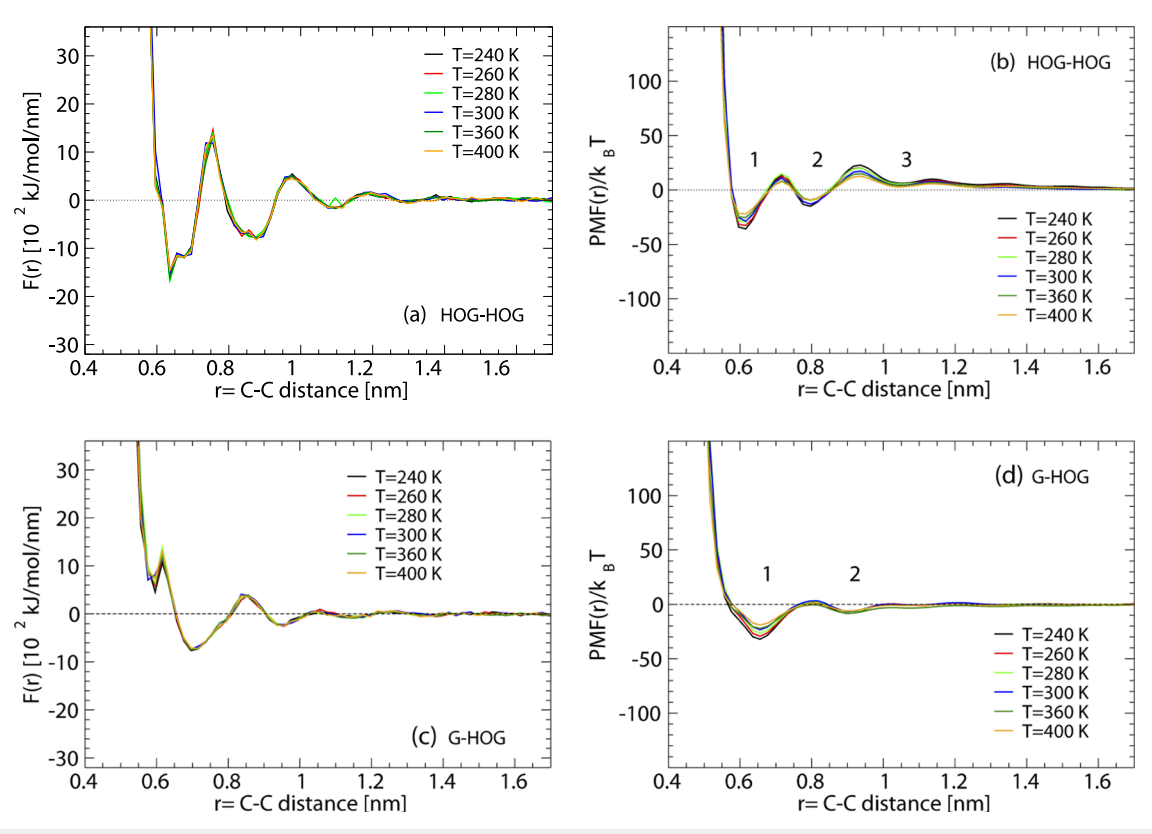


FIG. 3. Mean force and PMF as function of temperature (P = 0) for the case of (a) (b) two HOG-plates, and (c) (d) a pair of G-HOG plates. In both cases, the WMIs are barely sensitive to temperature. Numbers in (b) and (d) indicate the number of water layers formed between the plates at the plate separations corresponding to the PMF minima.

the hydrogen-bond (HB) network formed by the water molecules and the HOG-plates. It is possible that the lifetime and strength of the HB formed between the water molecules and the HOG-plates vary weakly with temperature. After all, the plates are located at fixed positions and, hence, they should be less affected by T-changes than, e.g., bulk water. This may explain the T-independence of the PMF between HOG-HOG and G-HOG plates at approximately r < 1.10 nm where only 1–3 water layers are accommodated in the confined space.

B. Enthalpic and entropic contributions

The temperature dependence of the PMF between two plates contains important information on the thermodynamic origin of the corresponding WMI. The PMF or, equivalently, the Gibbs free energy of the system at given (N, P, T) and plate separation r is given by G(r) = H(r) - TS(r), where H(r) and S(r) are the corresponding enthalpy and entropy of the system. In addition, it can be shown that the entropy is given by

$$S(r) = -\left(\frac{\partial G(r)}{\partial T}\right)_{P,N}.$$
 (1)

Hence, the temperature dependence of the PMF indicates whether the plates' PMF has an entropic contribution, i.e., given by the term -TS(r), and/or enthalpic component, i.e., given by the term H(r).

Next, we focus on the enthalpic and entropic contributions to the PMF for the three systems studied.

We estimate S(r) for the G-G, HOG-HOG, and HOG-G plate systems at T = 280 K. Following Ref. 36, we calculate S(r) by approximating Eq. (1) using

$$S(r) \approx -\left(\frac{G(r, T + \Delta T) - G(r, T)}{\Delta T}\right)_{PN}$$
 (2)

For a given system and plate separation r, we use Eq. (2) with $\Delta T = 20$ K and get an estimation for the entropy, $S_+(r)$. Similarly, by using Eq. (2) with $\Delta T = -20$ K, we get a second estimation for the entropy, $S_-(r)$. The entropies reported below are the corresponding average, $S_-(r) = \frac{S_+(r) + S_-(r)}{2}$.

We discuss, first, the hydrophobic case. Figure 4(a) shows the G(r) for the G-G plates at T=280 K together with the corresponding enthalpic H(r) and entropic -TS(r) contributions. At large separations (r>0.85 nm), $H(r)\leq 0$ while $-TS(r)\geq 0$. Accordingly, the metastable states where two $(r=r_2=0.93 \text{ nm})$ and three water layers $(r=r_3=1.31 \text{ nm})$ form between the plates are stabilized solely by enthalpic contributions. This is consistent with the view that, at $r=r_2, r_3$, water molecules can optimize the formation of water-water HB. In particular, the rather deep minimum of H(r) and maximum in -TS(r) at $r=r_2$ are due to the unique fully hydrogen-bonded structure adopted by bilayer water (see

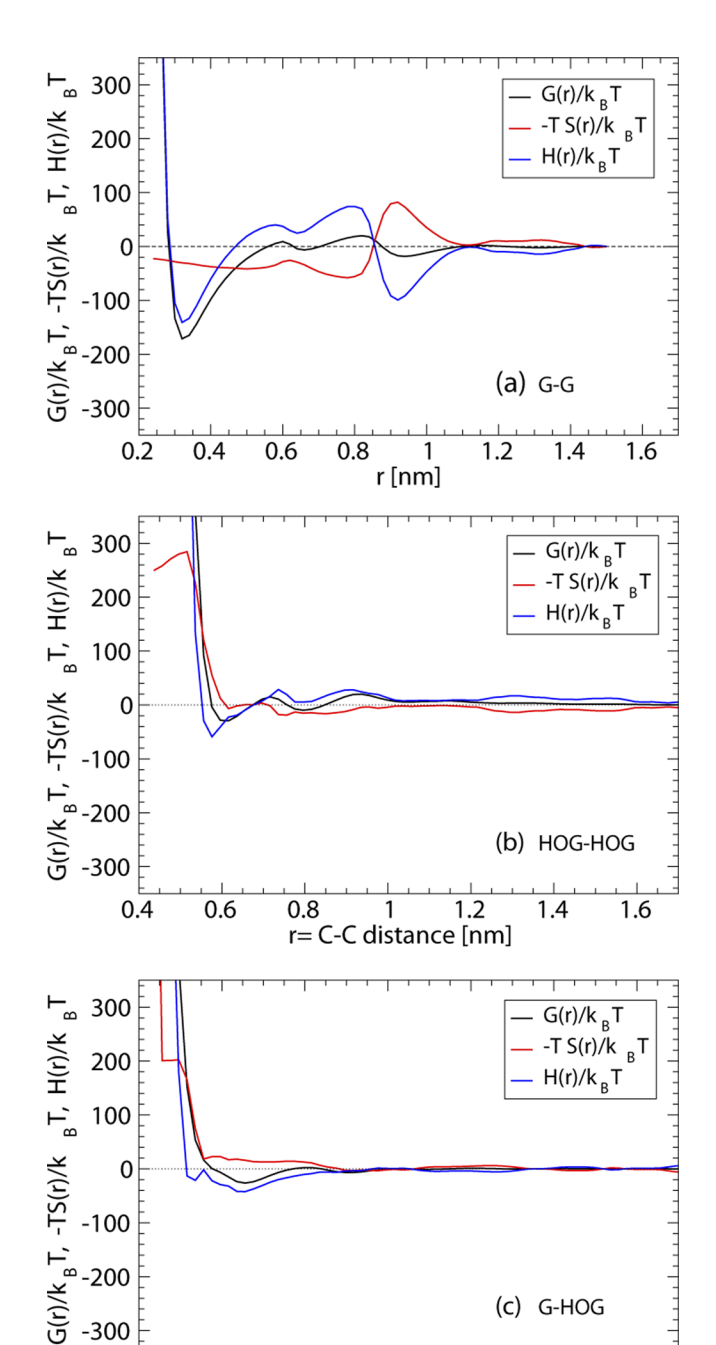


FIG. 4. Enthalpic [H(r)] and entropic [-TS(r)] contribution to the PMF [G(r) = H(r) - TS(r)] between pairs of plates at T = 280 K. (a) G-G, (b) HOG–HOG, and (c) G-HOG plates.

r= C-C distance [nm]

0.8

1.2

1.4

1.6

Refs. 24 and 25); at this plate separation, bilayer water forms a fully hydrogen-bonded structure that crystallizes rapidly (into a bilayer ice) at lower temperatures. 24,25

Figure 4(a) also shows that the local minimum of the PMF at $r = r_1 = 0.65$ nm (monolayer water) is stabilized due to entropic

contributions [-TS(r) < 0] while it is destabilized by enthalpic contributions [H(r) > 0]. This can be explained, again, by the formation of HB. Water molecules in a monolayer liquid configuration are expected to have broken HB, which explains the fact that H(r) > 0.37In addition, such molecules with broken HB are expected to be able to explore wider orientational motions than fully hydrogen-bonded water molecules, hence, explaining the negative entropic contributions to the PMF at $r = r_1$. The collapsed-plate state at $r = r_0 = 0.32$ nm is stabilized by both entropic and enthalpic contributions. The negative values of H(r) are due to the large plate-plate interactions at short separations which are attractive (<0). The entropic contributions at $r = r_0$ may be rationalized in terms of the water molecules expelled from the confined space, as the plates approach each other toward $r = r_0$. These molecules should be able to explore more molecular configurations when they belong to the bulk water reservoir than in a very tight water monolayer formed between the plates (at $r = r_0$).

We note that the enthalpic/entropic contributions shown in Fig. 4(a) are not necessarily general, valid to other hydrophobic plates, since they may vary with the plates' details and temperature (see results for the OG-OG plates in the supplementary material). For example, if the direct plate-plate interactions are less attractive at $r = r_0$ (while the plate–water interactions are left unchanged), the corresponding H(r) would increase (become less negative, or even positive) and the relative enthalpic/entropic contributions to the collapsed-plates state would change. For comparison, we note that the PMF between graphene plates at T = 298 K, and the corresponding enthalpic/entropic contributions, are reported in Ref. 38. Differently to our findings, it was found that the collapsed-plates state is stabilized solely by the entropic contribution [-TS(r) < 0]and destabilized by the enthalpic contribution [H(r) > 0]. Moreover, in that work, it was found that the monolayer water state $(r = r_1)$ was stabilized by enthalpy, the entropic contributions at these separations being relatively small. However, the plates employed in Ref. 38 ($\approx 1 \times 1 \text{ nm}^2$) are smaller than those used here $(\approx 2 \times 2 \text{ nm}^2)$. In addition, the plate-water interactions for the system considered in Ref. 38 are slightly different than ours. We also note that the entropic/enthalpic contributions to the WMI between hydrophobic surfaces vary with temperature³⁹ and surface details (e.g., Ref. 40). The results of Ref. 38 are obtained at higher temperature (T = 298 K) than ours (T = 280 K).

Next, we focus on the thermodynamic contributions to the PMF between HOG-HOG plates. Figure 4(b) shows the G(r), H(r), and -TS(r) for the HOG-HOG plates at T = 280 K. A comparison with Fig. 4(a) shows that both H(r) and -TS(r) are considerably smaller for the hydrophilic HOG-HOG plates than for the hydrophobic G-G plates. At plate separations r > 0.70 nm, -TS(r) ≤ 0 while H(r) > 0. This implies, e.g., that the metastable state at $r = r_2 = 0.80$ nm at which two water layers accommodate between the HOG-plates is stabilized by entropic contributions while enthalpic contributions tend to suppress this state. It is not evident why this is the case. The fact that H(r) > 0 at $r \approx r_2$ is probably due to a combination of (i) the direct electrostatic interactions between the plates and (ii) the ability of water molecules to form HB with other water molecules and the plates. Factor (i) is expected to increase H(r) since the silanol groups of one HOG-plate are in registry with the silanol groups of the opposite HOG-plate. Indeed, the PMF between two (uncharged) graphene plates decorated by

0.4

0.6

fixed, in-registry partial charges is repulsive due to positive enthalpic contributions. ⁴¹ The maxima in the PMF and H(r) at $r\approx 0.95$ nm and $r\approx 0.73$ nm are due to the disruption of HB among water molecules, as one layer of water molecules is expelled from the confined space when the plates move closer to one another, from r_n to r_{n-1} (n=3,2). That -TS(r)<0 at r>0.70 nm may be related to an increase in the orientational configurations (relative to the bulk) accessible to water molecules belonging to bilayer and trilayer water. For example, it may be possible that, at $r=r_2, r_3$, the surface silanol groups allow water molecules in the confined space to acquire orientational configurations not achievable in the bulk. Alternatively, the entropy of the system may increase because of water molecules being expelled from the confined space—water molecules in the reservoir may be able to explore larger orientational/translational motions.

At r < 0.70 nm, Fig. 4(b) shows that $-TS(r) \ge 0$. Instead, H(r) < 0 down to $r \approx 0.55$ nm, and then, it increases with decreasing r (due to the repulsive plate–plate interactions as $r \to 0$). It follows that the metastable state at $r = r_1 = 0.62$ nm, at which the plates are separated by one water layer, is stabilized solely by enthalpic contributions. This can be rationalized by the HB formed between the water monolayer and the plates. Water molecules are able to form HB with both the plates and other water molecules, lowering the potential energy/enthalpy of the system. Moreover, the HB between water and the plates should also limit the ability of water molecules to rotate and diffuse, which may reduce the entropy of the system $[-TS(r) \ge 0]$.

We conclude this section by discussing the G(r), H(r), and -TS(r) for the G-HOG plates at T = 280 K. As shown in Fig. 4(c), all three quantities are approximately zero for r > 1.0. The PMF for the G-HOG plates has a very mild minimum at $r = r_2 = 0.90$ nm at which two water layers accommodate between the plates. At this metastable state, H(r) and -TS(r) are slightly negative, meaning that the bilayer state is stabilized by both enthalpic and entropic contributions. The stable state at $r = r_1 = 0.65$ nm, at which the plates are separated by a water monolayer, is stabilized by enthalpic contributions [H(r) < 0] while entropic contributions tend to destabilize the system. This can be rationalized by the HB formed between the water monolayer and the HOG-plate. At $r = r_1$, water molecules are able to form HB with both the HOG-plate and the water molecules in the monolayer, lowering the potential energy/enthalpy of the system. However, the HB between the water molecules and the formation of HB between the HOG-plate and water should also limit the ability of water molecules to rotate and diffuse. This may explain the reduction in entropy [-TS(r) > 0] of the system

As for the hydrophobic plates, whether the hydrophilic and hybrid WMIs between the plates are enthalpic/entropic in origin is strongly dependent on the surface details, such as roughness and specific chemistry. For example, the decoration of the plates with large and mobile, polar molecules would affect the entropic contribution to the plates' PMF; see, e.g., Ref. 36. Hence, the results of Figs. 4(b) and 4(c) should be taken with caution and not generalized to other, more complex, surfaces.

C. Pressure-effects

The effects of pressure on the WMIs between G-G plates have been discussed in detail in Ref. 25. The mean force F(r) and PMF

between the G-G plates at different pressures and at T = 300 K are shown in Figs. 5(a) and 5(b). In the supplementary material, we compare the reported F(r) and PMF with those obtained in Ref. 25 using a Berendsen barostat with no graphene walls to control the pressure. The results from our simulations and those from Ref. 25 are fully consistent [see also Fig. 5(c) and discussion below].

Figure 5(a) shows that increasing the pressure enhances the oscillations of the mean forces between the plates. This leads to an increase in the activation free energy barriers ΔG_{act}^{ij} that the plates need to overcome in order to move from the plate separation $r = r_i$ to $r = r_j$ for $j = i \pm 1$ (i, j = 0, 1, 2, 3, 4) [Fig. 5(c)].⁴² Interestingly, all ΔG_{act}^{ij} values increase linearly with increasing pressure. Physically, these energy barriers ΔG_{act}^{ij} are associated to the process of adding (j=i+1) or removing (j=i-1) a water layer between the plates.²⁵ Accordingly, the increase of ΔG_{act}^{ij} upon compression makes such $r_i \rightarrow r_i$ transitions more difficult. We also note that the metastable local minima of the PMF, for n = 1, 2, 3, ..., become more stable upon compression. In the case of the collapsed-plate state (n = 0), compression up to $P \approx 1000$ MPa also increases the stability of this state of the system. However, further compression has the opposite effect and, at $P \approx 2025$ MPa, the collapsed-plate state vanishes, i.e., at such a high pressure, the plates will always be separated by at least one water layer. We note that the results from Ref. 25 for ΔG_{act}^{ij} at P = 0.1,400,800, and 1200 MPa are also included in Fig. 5(c). The agreement of these values (obtained using a Berendsen barostat) and our results [obtained by controlling the pressure using two external walls; see Fig. 1(b)] validates the methodology employed here to control the pressure of the system (see also the supplementary

Figure 6 shows the pressure-effects on the mean force, PMF, and activation energy barriers for the case of HOG-HOG plates. Increasing the pressure also affects the WMI between the HOG-HOG plates, particularly, at very short separations, approximately r < 0.9 nm. Interestingly, pressure removes the PMF minimum located at $r = r_2 \approx 0.80$ nm. This local minimum corresponds to a metastable state where there are two water layers between the plates. Accordingly, at very high pressures, the plates may only transition between the stable state of the system, corresponding to $r = r_1$ = 0.62 nm (n = 1 water layer between the plates), and the metastable state of the system corresponding to $r = r_3 = 1.05$ nm (n = 3 water layers between the plates). Consistent with these observations, the activation free energies ΔG_{act}^{ij} with i = 2 and j = 1,3 decrease with increasing pressure and vanish at $P \approx 1500$ MPa. The rest of the activation energy barriers increase upon compression, as found for the case of G-G plates. We also note that the stable state of the system (corresponding to $r = r_1$) becomes more stable (more negative PMF) with increasing pressures.

The effects of increasing pressure on the F(r) and PMF between the G-HOG plates are shown in Figs. 7(a) and 7(b). As for the G-G plates, the oscillations of both F(r) and G(r) become more pronounced with increasing pressure. In particular, all the activation free energies ΔG_{act}^{ij} increase linearly with increasing P [Fig. 7(c)]. Accordingly, increasing pressure stabilizes the stable/metastable states that accommodate n=1,2,3,4 water layers between the plates. Interestingly, none of these metastable/stable states is removed (destabilized) upon compression. As for the case of the HOG-HOG plates system, and contrary to the case of the G-G plates, the stable

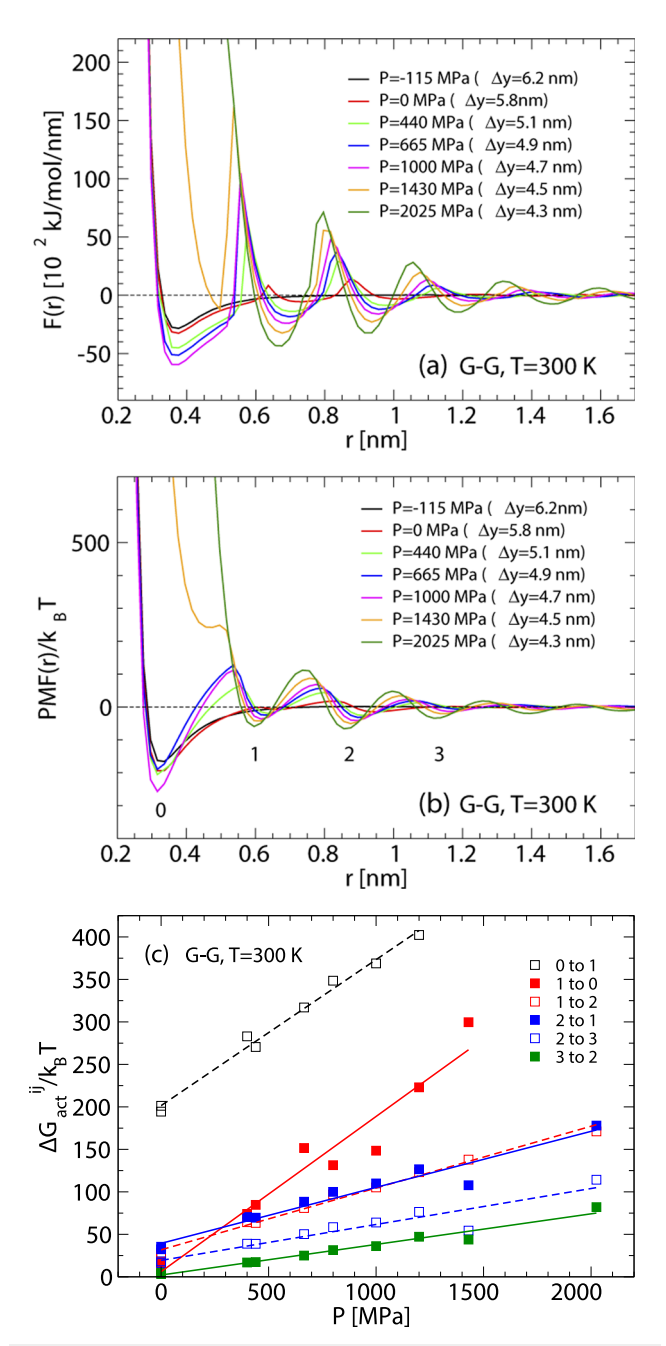


FIG. 5. (a) Mean force and (b) PMF between G-G plates immersed in water at selected pressures ($T=300\,$ K). Numbers in bold font in (b) indicate the number of water layers formed between the plates at the separations corresponding to the PMF minima. (c) Activation free energies ΔG^{ij}_{act} obtained from (b). ΔG^{ij}_{act} is the free energy barrier corresponding to the process of changing the plate separation from r_i to r_j ($j=i\pm1$), where r_i is the location of the ith minima of the total PMF. i and j are given in the figure labels. In all cases, the activation free energies increase upon compression, disfavoring (i.e., making kinetically more difficult) the collapse of the graphene plates. Results for P=0.1, 400, 800, 1200 MPa are from Refs. 25. The stable collapsed-plate state corresponding to the PMF minimum at $r=r_0\approx0.30\,$ nm becomes unstable at $\sim>1430\,$ MPa.

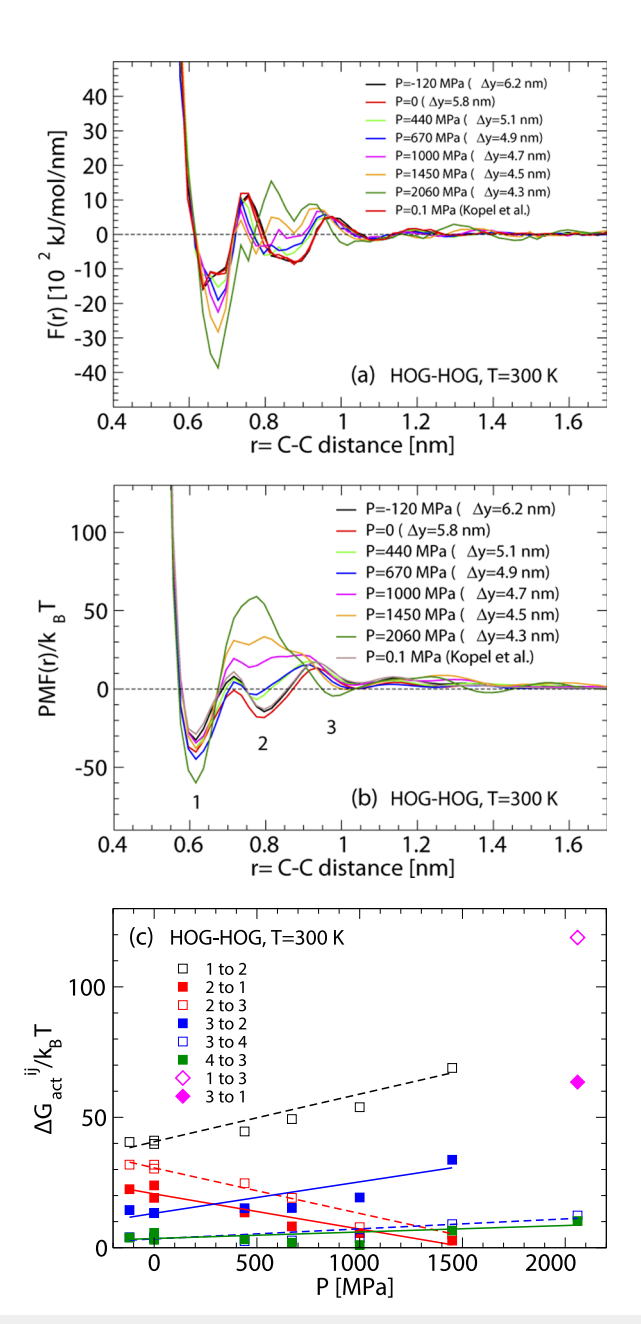


FIG. 6. (a) Mean force and (b) PMF between HOG-HOG plates immersed in water at selected pressures ($T=300~{\rm K}$). Numbers in bold font in (b) indicate the number of water layers formed between the plates at the separations corresponding to the PMF minima. (c) Activation free energies ΔG^{ij}_{act} obtained from (b). At $P\approx 1500~{\rm MPa}$, the metastable state corresponding to $r_2=0.80~{\rm nm}$ becomes unstable and $\Delta G^{21}_{act}=\Delta G^{23}_{act}\to 0$ (red squares). At $P>1500~{\rm MPa}$, a single free energy barrier separates the stable/metastable states corresponding to $r_1=0.62~{\rm nm}$ and $r_3\approx 1.05~{\rm nm}$ (magenta diamonds).

state (corresponding to $r = r_1$) becomes more stable (more negative PMF) upon compression.

It may be somewhat unexpected that the bilayer water configuration confined by HOG-HOG becomes unstable at high pressures.

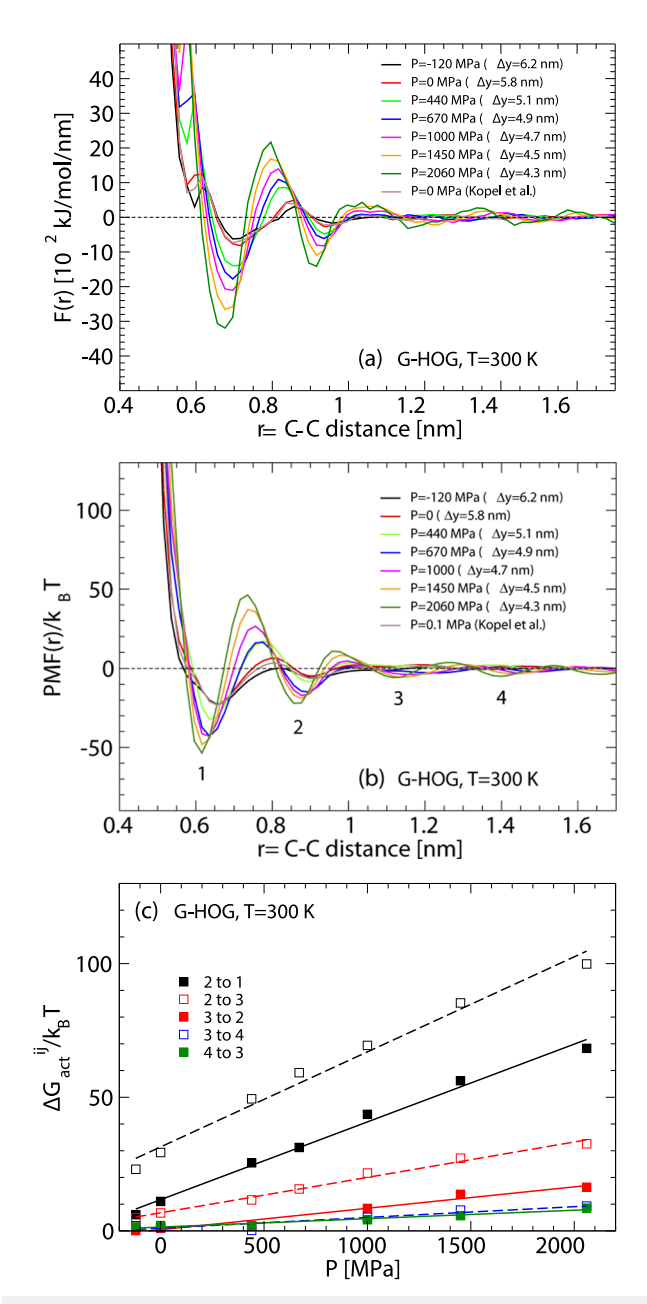


FIG. 7. (a) Mean force and (b) PMF between G-HOG plates immersed in water at selected pressures ($T=300~{\rm K}$). Numbers in bold font in (b) indicate the number of water layers formed between the plates at the separations corresponding to the PMF minima. (c) Activation free energies ΔG^{ij}_{act} obtained from (b). In all cases, the energy barriers increase upon compression, disfavoring (i.e., making kinetically more difficult) the collapse of the graphene plates.

This can be rationalized by noticing that when bilayer water is confined between HOG-HOG plates, the water molecules must form HB with their closest plate and with other water molecules. This can be problematic as more and more water molecules are pushed

into the confined space when the pressure increases. Our results suggest that at high pressures (approximately $P>1450~{\rm MPa}$), there are too many water molecules between the HOG-HOG plates so that the HB network among the water molecules and surface OH groups becomes disrupted, making the bilayer water state energetically unfavorable. In the case of HOG-G plates, only one water layer can form HB with the HOG-plate. This constrains the orientational degrees of freedom of the water molecules that are located next to the HOG-plate. However, the water molecules in the opposite water layer, next to the G-plate, are not constrained by the formation of HB with the G-plate, and hence, they can rotate in order to maintain the HB network in the whole confined space even at high pressures.

Overall, our results indicate that hydrophobic, hydrophilic, and hybrid WMIs are all sensitive to pressure. However, we stress that the changes induced by pressure are weaker for the hydrophilic and hybrid cases than for the hydrophobic case. Specifically, changes in the values of ΔG_{act}^{ij} are as large as $\delta(\Delta G_{act}^{ij}) \approx 300 \text{ k}_B\text{T}$ for the G-G plates [Fig. 5(c)] and $\delta(\Delta G_{act}^{ij}) \approx 100 \text{ k}_B\text{T}$ for the HOG-HOG and G-HOG plates [Figs. 6(c) and 7(c)]. In other words, the presence of at least one hydrophilic surface strongly suppresses the sensitivity to pressure of the WMIs between the plates.

IV. SUMMARY AND CONCLUSIONS

In this work, we perform extensive MD simulations to study the WMIs between flat, nanoscale graphene-based surfaces. The aim of this work is to compare the T- and P-effects on the WMIs between (i) two graphene plates (hydrophobic interactions), (ii) two hydroxylated graphene plates (hydrophilic interactions), and (i) between a hydroxylated graphene and a graphene plate (hybrid interactions). We found that all three kinds of WMIs vary with pressure but, while the hydrophobic interactions are considerably affected by T-changes [case (i)], hydrophilic and hybrid WMIs [cases (ii) and (iii)] are practically T-independent. In all cases, the main effect of increasing the pressure is to increase the free energy barriers separating the local minima of the corresponding PMF (these minima correspond to metastable states at which water molecules are able to arrange in layers between the plates). Interestingly, in a few cases, the metastable plate separation becomes unstable at very high pressures. Isobaric cooling tends to increase the free energy barriers separating the metastable plate separations.

The effects of temperature on the WMIs between the different pair of plates studied are particularly interesting. The practically lack of T-effects on the WMIs in cases (ii) and (iii), which is contrary to the (non-negligible) T-effects found on the WMI in case (i), implies that a single hydrophilic plate is sufficient to induce hydrophilic-like WMI. In other words, a hydrophilic plate imposes its nature to an opposite hydrophobic plate. From a microscopic point of view, this can be understood by noticing that an HOG-plate is able to "pin" (temporarily) interfacial water molecules via the formation of hydrogen bonds, favoring the retention of water molecules between the plates as the temperature varies. ⁴³ Instead, hydrophobic plates tend to enhance the density fluctuations of interfacial water. ^{44,45} Macroscopically, hydrophobic surfaces tend to increase

the water compressibility and thermal expansion coefficient while hydrophilic surfaces do not. 46,47 This explains why the hydrophobic WMIs are much more sensitive to T than hydrophilic/hybrid WMIs

The results of this work are important for our fundamental understanding of self-assembly processes in aqueous environments, including protein denaturation, interactions between biomolecules (e.g., protein aggregation), and WMIs between nanoparticles, and how such processes may be affected by changes in the working conditions (T and P). For example, the finding that T mostly affects hydrophobic interactions suggests that *T*-induced protein denaturation may originate in the interactions between hydrophobic residues or domains. Instead, P-induced protein denaturation is probably related to changes of the WMIs between hydrophobic-hydrophobic, hydrophilic-hydrophilic, and hydrophobic-hydrophilic pair of residues or domains. From a computational point of view, our study suggests how implicit water models should be modified to take into consideration the effects of T and P on the WMIs between nanoscale hydrophobic-hydrophobic, hydrophilic-hydrophilic, and hydrophobic-hydrophilic pairs of surfaces; see, for example, Ref. 29. Our results are based on atomically smooth, hydrophilic (HOG-plates) and weakly hydrophobic (G-plates) surfaces. An important issue to address in the future is how these results are affected when very hydrophobic surfaces and surfaces with a complex molecular structure are considered. In such cases, water confined by hydrophobic walls may remain metastable at small separations and evaporation of water between the confining plates may occur (see the supplementary material). In such cases, the kinetics of evaporation can play a relevant role with practical implications^{32–34,48} (see the supplementary material).

SUPPLEMENTARY MATERIAL

See the supplementary material for (i) additional tests of the method used in this work to control the pressure of the system; (ii) the temperature-effects on the PMF between (apolar) OG-OG plates and the corresponding enthalpic and entropic contributions; and (iii) additional MD simulation results addressing the potential metastability of confined water at the small plate separations.

ACKNOWLEDGMENTS

Support for this project was provided by the National Science Foundation (NSF; Grant No. CBS-1604504), the NSF CREST-IDEALS Center (Grant No. HRD-1547380), and a PSC-CUNY Award, jointly funded by The Professional Staff Congress and The City University of New York. This research was supported, in part, by a grant of computer time from the City University of New York High Performance Computing Center under NSF Grant Nos. CNS-0855217, CNS-0958379, and ACI-1126113.

AUTHOR DECLARATIONS

Conflict of Interest

The authors have no conflicts to disclose.

Author Contributions

Justin Engstler: Data curation (equal); Formal analysis (equal); Writing – review & editing (equal). **Nicolas Giovambattista:** Data curation (equal); Formal analysis (equal); Writing – review & editing (equal).

DATA AVAILABILITY

The data that support the findings of this study are available within the article and its supplementary material.

REFERENCES

- ¹D. Thirumalai, G. Reddy, and J. E. Straub, Acc. Chem. Res. 45, 83–92 (2012).
- ²D. E. Scott, A. R. Bayly, C. Abell, and J. Skidmore, Nat. Rev. Drug Discovery 15, 533–550 (2016).
- ³C. Tanford, *The Hydrophobic Effect: Formation of Micelles and Biological Membranes* (Wiley, New York, 1980).
- ⁴J. A. Long, B. M. Rankin, and D. Ben-Amotz, J. Am. Chem. Soc. 137, 10809–10815 (2015).
- ⁵ Structure and Dynamics of Membranes, Handbook of Biological Physics, edited by R. Lipowsky and E. Sackmann (Elsevier, Amsterdam, 1995).
- ⁶E. Shakhnovich, Chem. Rev. 106, 1559–1588 (2006).
- ⁷A. Ben-Naim, *The Protein Folding Problem and Its Solutions* (World Scientific, Singapore, 2013).
- ⁸L. Young, R. L. Jernigan, and D. G. Covell, Protein Sci. 3, 717–729 (1994).
- ⁹Y. Levy and J. N. Onuchic, Annu. Rev. Biophys. Biomol. Struct. **35**, 389-415 (2006).
- ¹⁰E. Xi, V. Venkateshwaran, L. Li, N. Rego, A. J. Patel, and S. Garde, Proc. Natl. Acad. Sci. U. S. A. 114, 13345–13350 (2017).
- ¹¹D. Chandler, Nature **437**, 640–647 (2005).
- ¹²D. Ben-Amotz, "Water-mediated hydrophobic interactions," Annu. Rev. Phys. Chem. 67, 617–638 (2016).
- ¹³N. B. Rego, X. Erte, and A. J. Patel, Proc. Natl. Acad. Sci. U. S. A. 118, e2018234118 (2021).
- ¹⁴ A. Ben-Naim, J. Chem. Phys. **90**, 7412–7425 (1989).
- ¹⁵ A. Ben-Naim, J. Chem. Phys. **93**, 8196–8210 (1990).
- ¹⁶ A. Ben-Naim, J. Phys. Chem. A **125**, 024901 (2006).
- ¹⁷S. R. Durell and A. Ben-Naim, <u>Biopolymers</u> **107**, e23020 (2017).
- ¹⁸D. Mallamace, S.-H. Chen, C. Corsaro *et al.*, Sci. China Phys., Mech. Astron. **62**, 107003 (2019).
- ¹⁹Y. Kopel and N. Giovambattista, J. Phys. Chem. B **123**, 10814–10824 (2019).
- ²⁰M. Kanduč and R. R. Netz, Proc. Natl. Acad. Sci. U. S. A. 112, 12338–12343 (2015).
- ²¹ M. Kanduč, A. Schlaich, E. Schneck, and R. R. Netz, Langmuir 32, 8767–8782 (2016).
- ²² A. Ben-Naim, J. Phys. Chem. **94**, 6893–6895 (1990).
- ²³ N. Giovambattista, P. J. Rossky, and P. G. Debenedetti, Annu. Rev. Phys. Chem. 63, 179–200 (2012).
- ²⁴J. Engstler and N. Giovambattista, J. Phys. Chem. B **122**, 8908–8920 (2018).
- ²⁵J. Engstler and N. Giovambattista, J. Phys. Chem. B **123**, 1116–1128 (2018).
- ²⁶D. Paschek, S. Hempel, and A. E. García, Proc. Natl. Acad. Sci. U. S. A. 105, 17754–17759 (2008).
- ²⁷S. B. Kim, J. C. Palmer, and P. G. Debenedetti, Proc. Natl. Acad. Sci. U. S. A. 113, 8991–8996 (2016).
- $^{\mathbf{28}}\text{H}.$ Herberhold and R. Winter, Biochemistry 41, 2396–2401 (2002).
- ²⁹B. J. Sirovetz, N. P. Schafer, and P. G. Wolynes, J. Phys. Chem. B 119, 11416–11427 (2015).
- ³⁰ J. L. F. Abascal and C. Vega, J. Chem. Phys. 123, 234505 (2005).
- ³¹ F. W. Starr, F. Sciortino, and H. E. Stanley, Phys. Rev. E **60**, 6757 (1999).
- ³²S. Sharma and P. G. Debenedetti, Proc. Natl. Acad. Sci. U. S. A. **109**, 4365 (2012).
- ³³ K. Leung, A. Luzar, and D. Bratko, Phys. Rev. Lett. **90**, 065502 (2003).

- ³⁴ A. Luzar, J. Phys. Chem. B **108**, 19859 (2004).
- 35 B. Hess, C. Kutzner, D. van der Spoel, and E. Lindahl, J. Chem. Theory Comput. 4, 435–447 (2008).
- ³⁶C. Eun and M. L. Berkowitz, J. Chem. Phys. **136**, 024501 (2012).
- ³⁷N. Giovambattista, P. G. Debenedetti, and P. J. Rossky, J. Phys. Chem. B 111, 9581 (2007).
- ³⁸N. Choudhury and B. M. Pettitt, J. Phys. Chem. B **110**, 8459 (2006).
- ³⁹ R. Zangi and B. J. Berne, J. Phys. Chem. B **112**, 8634 (2008).
- ⁴⁰ A. Wallqvist and B. J. Berne, J. Phys. Chem. **99**, 2893 (1995).
- ⁴¹ L. Lu and M. L. Berkowitz, J. Chem. Phys. **124**, 101101 (2006).
- ⁴²Figure 5(c) includes data from Ref. 25 for P = 0.1, 400, 800, 1200 MPa. Since the area of the G-plates used in Ref. 25 is $A' = 1.709 \times 1.762 \text{ nm}^2$, smaller than
- the plates area employed in this work ($A=1.832\times1.974~\mathrm{nm}^2$), the results from Ref. 25 in Fig. 5(c) are rescaled by a factor A/A'=1.20.
- ⁴³ N. Giovambattista, P. G. Debenedetti, and P. J. Rossky, J. Phys. Chem. C 111, 1323 (2007).
- ⁴⁴ A. J. Patel, P. Varilly, and D. Chandler, J. Phys. Chem. B **114**, 1632–1637 (2010).
- ⁴⁵H. Acharya, S. Vembanur, S. N. Jamadagni, and S. Garde, Faraday Discuss. **146**, 353–365 (2010).
- ⁴⁶N. Giovambattista, P. J. Rossky, and P. G. Debenedetti, Phys. Rev. E 73, 041604 (2006).
- ⁴⁷N. Giovambattista, P. J. Rossky, and P. G. Debenedetti, J. Phys. Chem. B **113**, 13723–13734 (2009).
- ⁴⁸P. G. Bolhuis and D. Chandler, J. Chem. Phys. 113, 8154 (2000).